UC Irvine
UC Irvine Previously Published Works

Title
Microfluidic dielectrophoretic sorter using gel vertical electrodes

Permalink
https://escholarship.org/uc/item/4n48v055

Journal
Biomicrofluidics, 8(3)

ISSN
1932-1058

Authors
Luo, Jason
Nelson, Edward L
Li, GP
et al.

Publication Date
2014-05-01

DOI
10.1063/1.4880244

Peer reviewed

eScholarship.org Powered by the California Digital Library
University of California

Microfluidic dielectrophoretic sorter using gel vertical electrodes

Jason Luo,[1,a)] Edward L. Nelson,[2] G. P. Li,[3] and Mark Bachman[1,3]
[1]*Department of Biomedical Engineering, University of California, Irvine, California 92697, USA*
[2]*Department of Medicine, Institute for Immunology, University of California, Irvine, California 92697, USA*
[3]*Department of Electrical Engineering and Computer Science, University of California, Irvine, California 92697, USA*

(Received 28 March 2014; accepted 16 May 2014; published online 23 May 2014)

We report the development and results of a two-step method for sorting cells and small particles in a microfluidic device. This approach uses a single microfluidic channel that has (1) a microfabricated sieve which efficiently focuses particles into a thin stream, followed by (2) a dielectrophoresis (DEP) section consisting of electrodes along the channel walls for efficient continuous sorting based on dielectric properties of the particles. For our demonstration, the device was constructed of polydimethylsiloxane, bonded to a glass surface, and conductive agarose gel electrodes. Gold traces were used to make electrical connections to the conductive gel. The device had several novel features that aided performance of the sorting. These included a sieving structure that performed continuous displacement of particles into a single stream within the microfluidic channel (improving the performance of downstream DEP, and avoiding the need for additional focusing flow inlets), and DEP electrodes that were the full height of the microfluidic walls ("vertical electrodes"), allowing for improved formation and control of electric field gradients in the microfluidic device. The device was used to sort polymer particles and HeLa cells, demonstrating that this unique combination provides improved capability for continuous DEP sorting of particles in a microfluidic device. © *2014 AIP Publishing LLC*.
[http://dx.doi.org/10.1063/1.4880244]

I. BACKGROUND

Microfluidic techniques and devices have shown much ability in recent years for the sorting and identifying of nano- to microscale particles.[1–8] Dielectrophoresis (DEP) is a common microfluidic technique which accomplishes this using electric field gradients.[9–17] This has been applied to various biomedical assays, such as rare cell detection, protein separation, and enrichment of a cell population of interest.[18–25] Traditionally, the electric field gradient necessary for DEP is formed in a microchannel using two-dimensional electrodes strategically patterned on the device substrate.[19] The field tends to be strongest at the edges of these planar electrodes, and weaker in between them. Additionally, electric field strength dissipates as the field lines extend away from the electrodes and disperse over a larger volume.[26] Together, this forms the gradient for exerting the DEP force on passing particles.

Recently, interest has grown in more precisely refining and optimizing all three dimensions of these field gradients.[27–35] Vertical electrodes are one such development in this technology.[26,36,37] By expanding on various photolithographic techniques, these electrodes are cast into the walls of microfluidic channels and project vertically uniform electric fields spanning the

[a)]Email: jtluo@uci.edu

 © 2014 AIP Publishing LLC

microchannel when an electric potential is applied. Vertical electrode devices avoid the two main complications associated with most DEP devices constructed with planar electrodes. Planar electrodes tend to separate particles either by repelling them away from, or trapping them to, the electrodes, making retrieval of sorted particle batches a challenge, necessitating either that the user collect fractions from the outlet[38] or that the device be switched on and off to collect particles caught at the electrodes' edges.[39] Second, in devices utilizing planar electrodes, the electric field gradient can dissipate dramatically as the field lines move away from the electrodes such that particles entering the device near the channel ceiling experience a negligible DEP force.[40] With vertical electrodes spanning the height of the device, one dimension is invariant, effectively creating a continuously operable two-dimensional particle separation profile, eliminating any dead zones and streamlining the particle sorting and retrieval processes.[41]

Finally, efficient DEP sorting requires that particles enter the sorter in a focused stream to avoid the variability in DEP forces across a microchannel that can result in smearing and compromising separation efficiency.[41,42] Because the field gradient is strongest along one channel sidewall and weakest along the other, were particles to enter the device randomly distributed across the width of the channel, those nearest the strong side might experience a disproportionately large force while those who happen to flow through the weak side might experience little or no DEP force at all. To alleviate this, in the device presented, particles are continuously focused into a narrow stream using two rows of microposts. In this filter-like system, particles above a pre-set diameter are gently swept toward a consolidated flowline until, immediately prior to entering the DEP sorting region, the particles are arranged in a narrow band and consequently experience essentially identical exposure to the electric field gradient and the resultant DEP force is exclusively the result of the particle's physical properties. The net result is a continuously operable particle sorting system that can sort particles indefinitely without any user input beyond the initial setup and final recovery of particles.

II. OPERATING PRINCIPLE

A. Pre-focusing

As noted immediately above, efficient sorting of particles by lateral dielectrophoresis mandates that each particle passes through the DEP section of the device along the same flowline. Under the low Reynolds number conditions found in microfluidic devices, particles are difficult to rearrange or shift into different flow lines.[43] Hydrodynamic focusing is often used to generate a narrow stream of particles, such as in a flow cytometer. In such a strategy, separate streams of fluid (sheath flow) are brought in to pinch a main flow stream, resulting in a narrow band of flow.[44,45] However, this requires the use of a separate flow, and carefully controlled flow rates, adding significant complexity to the system. Several techniques for creating a narrow stream of particles in a microfluidic device have been described including taking advantage of laminar flow properties,[43,46] simultaneously exposing particles to multiple forces, e.g., gravity in field-flow fractionation,[12,20,47,48] or a second electric field gradient such as in earlier 3-D electrode devices,[41] thereby forcing the particles to settle into equilibrium streamlines. In the presented device, we have demonstrated efficient passive focusing via an elegant, continuous-flow micropillar system. This focusing apparatus forces incoming particles to enter the DEP device along a narrow stream approximately one particle diameter wide using only laminar flow principles and particle size as drivers for the focusing.

In our micropillar system, rows of pillars spanning height of the channel are cast into the inlet channel of the device, spaced several microns apart. Exact sizes for the pillars and gaps can be designed for specific particle suspensions. The row of pillars is angled relative to the direction of fluid flow such that it disrupts but does not impede the movement of particles. Theoretically, row angle can range from 0°, i.e., parallel to flow, in which case it exerts no effect, up to 90°, in which case it would act as a traditional size-based filter, completely immobilizing all incoming particles above a certain diameter. In actuality, the angle is very near parallel with fluid flow: in this configuration, buffer and particles below the size threshold pass through the gaps between posts while particles too big to fit through the gaps are nonetheless

able to continue along the direction of fluid flow, skimming along the row of pillars. By carefully tuning row angle and gap size, as well as the position of the micropillar row within the microfluidic channel, it is thus possible to gently guide larger particles into a tight stream for collection or further processing downstream. Additionally, the synchronous use of two or more such micropillar rows can effectively direct particles into a flow stream located at any position across the width of the channel and to repeatedly redirect a particle line in the same device. A limited number of variations to this technology has seen application in redirecting particles into different laminar flowstreams, in general, as well as in shuttling them back and forth through various reagents for strategically applying various coatings in a layer by layer process.[49–51] Our use of this focusing step is for the improvement of the DEP separation process.

B. Dielectrophoretic particle separation

A detailed presentation on dielectrophoresis theory is beyond the scope of this paper; instead, a brief synopsis is presented to cover the use of this phenomenon for microparticle separation. When exposed to a non-uniform AC electric field, microscale particles such as polystyrene beads or mammalian cells can polarize and experience translational forces despite their lack of permanent charge,[52–54] as the pole nearer the field maxima experiences a force stronger than that felt by its opposing pole towards the field minima. The direction of this force depends on the particle's polarizability relative to that of the medium: if the particle is more polarizable than the medium it will migrate up the field gradient (positive dielectrophoresis, or pDEP), while if it is less polarizable it will migrate down (negative dielectrophoresis, or nDEP).[55,56] The basis of dielectrophoretic detection and sorting, then, lies in tuning the frequency and voltage of the applied signal as well as the conductivity of the buffer such that at a certain configuration, each particle type in a given suspension experiences a DEP force sufficiently different from that experienced by particles of every other type.[10,20] Because the DEP force depends on various factors, many of which are intrinsic to the particle, including the particle size, polarizability, and speed of polarization alignment, DEP is a useful tool for probing differences among particles with different dielectric properties, primarily through physical sorting based on the forces associated with DEP.[57–61]

For homogeneous spherical particles, the dielectric force is governed by

$$\vec{F}_{DEP} = 2\pi r^3 \varepsilon_m Re(CM) \vec{\nabla} |\vec{E}|^2, \tag{1}$$

where r is the particle radius, ε_m is the permittivity of the media, *Re(CM)* is the real component of the Clausius-Mossotti relation, and $\vec{\nabla}|\vec{E}|^2$ is the gradient of the square of the electric field. The Clausius-Mossotti relation is expressed as the following:

$$\frac{\varepsilon_p^* - \varepsilon_m^*}{\varepsilon_p^* + 2\varepsilon_m^*}, \tag{2}$$

where

$$\varepsilon^* = \varepsilon - \frac{\sigma}{i\omega} \tag{3}$$

and summarizes the relationship between the polarizabilities of the dielectric particles and the suspending medium.[18] The real component of the Clausius-Mossotti factor ranges from $-\frac{1}{2}$ for particles much less polarizable than the medium to $+1$ for the opposite case. Thus, while particle size and strength of the electric field as well as the steepness of the gradient contribute towards the magnitude of the dielectrophoretic force, it is the particles' electronic properties that ultimately determine the direction of the force.[60]

Finally, at the microfluidic scale, resisting this dielectrophoresis force is a substantial drag force governed by Stokes's Law; particles reach terminal velocity when these two forces balanced, which for spherical particles is expressed as

$$v = \frac{\vec{F}_{DEP}}{6\pi\eta r} = \frac{2\pi r^2 \varepsilon_m Re(CM)\vec{\nabla}|\vec{E}|^2}{6\pi\eta}, \tag{4}$$

where η is the viscosity of the suspending medium.[60] Thus, lateral DEP separation functions primarily due to different particles arriving at different lateral terminal velocities: as particles travel downstream in the direction of flow, they shift laterally at different speeds, and find themselves in varying flowstreams leading up to the device exit. Assuming all particles started along the same flowstream, particles are thus grouped into flowstreams based on their physical and electronic properties, and can thus be shunted into different outlets as sorted batches. Our device utilizes this approach by first injecting particles in a narrow stream before performing DEP separation. This approach is similar to DEP field flow fractionization which often results in distinct flow streams of different particles. However, in this approach, we separate particles in the lateral direction and rely on laminar flow to keep particles in their streams. Our approach does not attempt to balance two externally applied forces (e.g., gravity and DEP) to produce distinct particle streams.

C. Gel vertical electrodes

Photolithographic techniques for the fabrication of microfluidic devices that include vertical electrodes can be challenging. Proposed alternatives include DEP devices employing various forms of insulating barriers to sculpt the electric field; these DEP devices are known as insulator-based dielectrophoresis (iDEP), electrodeless dielectrophoresis (eDEP), or contactless dielectrophoresis (cDEP) devices.[58,62–68] In cDEP devices, planar electrodes are isolated from the main flow channel by thin polydimethylsiloxane (PDMS) walls. When the device is activated, field lines emanate from the electrodes towards the walls: these thin walls then translate these field lines into a vertically uniform electric field in the main channel via their capacitive properties.[62,63] iDEP/eDEP devices are comparable in that electric field lines emanate generally consist of two-dimensional electrodes that inject field lines into the channels. However, these field lines are not separated from the main channel via any walls and are instead projected directly into the main channel. They are, however, sculpted using insulating features cast in the channels; the fields are thus forced to expand and contract in specific positions, yielding a precisely shaped gradients typically aligned orthogonal to the direction of flow to yield lateral DEP sorting.[64,69,70]

The gel electrodes presented here are a fusion of microfabricated vertical electrode DEP and iDEP. Using a conductive liquid that cools into a semisolid, it is possible to take advantage of laminar flow techniques to direct the hot material in liquid form into a microfluidic device and to deposit the hot liquid into strategically placed segments, which rapidly cools into a durable gel structure that resists deformation and flow. Thus, a solid conductive material can be precisely patterned in the device without the use of any difficult cleanroom fabrication techniques.

Finally, the electrodes in the insulator-based DEP devices are by definition separate from the medium; because voltage dissipates as electric field lines travel through the various elements of the device towards to particles of interest, this necessitates the use of large voltage differences across the planar electrodes in order to generate a sufficient field gradient for particle sorting. Conductive materials such as saline gels effectively transfer field lines towards the particles with minimal voltage drops in the electrodes themselves, thus reducing the power required to perform a similar particle separation. Thus, the design presented herein provides additional advantages over previously proposed iDEP designs to improve lateral DEP sorting.[71,72]

III. METHODS AND MATERIALS

The device combines both passive focusing and active dielectrophoretic sorting. As shown in Figure 1, it consists of an inlet, a focuser that serves to concentrate all incoming particles into a tight stream, an electronic component that sorts particles by type, and a trifurcation that

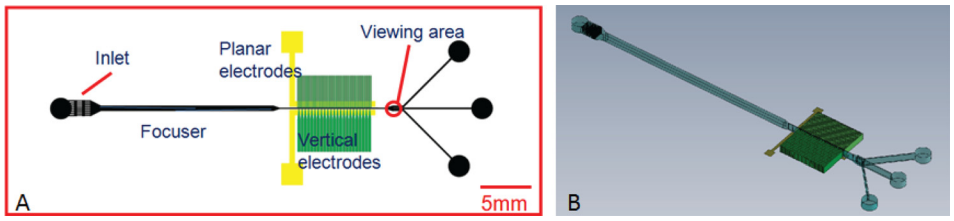

FIG. 1. Panel (a): Device schematic, to scale. Particles enter through the inlet into the PDMS microchannel (black). Particles pass through focusing region and are focused into a tight stream at the centerline of the flow channel before entering the DEP sorting region. AC potential applied through the planar electrodes is transferred by the vertical gel electrodes (green) into the main channel. Signals deflect particles, which then exit through one of three outlets. Particles that experience nDEP exit through the lowermost channel while particles that experience pDEP deflection exit through the uppermost. Separation depends on calibrating the signal such that particles of different type exit through different channels. Panel (b): Representative schematic (relative heights distorted for visualization) of device layers and vertical electrode geometry. Actual channel height: 50 μm.

separates the particles into sorted batches for retrieval. The device is cast in PDMS (Ellsworth Adhesives, Germantown, WI) and aligned over planar Au/Ti electrodes, which are in turn wired to an external electronic AC generator. The PDMS channels are sealed to the electrodes via an acrylic manifold; the bulk particle suspension is connected to the device via this manifold and is itself driven by an external syringe pump.

A. Numerical simulations

Device geometry was guided using coupled physics simulations that combined the results of finite element modeling of fluids and electric fields with transport simulations of particles subject to forces that result from flow and DEP. All geometries for the simulations were prepared using SolidWorks (Waltham, MA, USA) and then exported to the appropriate numerical package for calculations. The simulations consisted of three steps. First, the electric field was numerically calculated in 2D using COMSOL's finite element solver, using the Laplace equation with Dirichlet-conditions on the electrode edges and homogeneous Neumann-conditions on the outer boundary. Second, the flow of the water was numerically calculated in 2D using COMSOL's finite element solver, using the Navier-Stokes equation for incompressible fluid, and non-slip conditions at the boundary and fully developed flow at the inlet and outlet. Third, custom transport code was written in Python to calculate forces on small particles using (a) known DEP force equations (see below), and (b) drag forces using Stokes's law, and transport them through the system. The real component of the Clausius-Mossotti factor was calculated in the code using known conductivities and dielectric values for the particles' and buffer. The transport algorithm used both the COMSOL fluid flow results and COMSOL electric field results to determine the forces on the particles at each time step. In addition, the transport algorithm checked to ensure that particles could not pass into regions that were geometrically impossible, such as through the small openings of the sieve (if they were too large). 2D modeling assumes a high aspect ratio channel and underestimates spread caused by particles flowing near the top and bottom of the channel. DEP and Stokes forces were calculated using materials properties for particles of various size and material, from 6 μm erythrocytes and 20 μm tumor cells to 15 μm polystyrene spheres. The purpose of this modeling effort was to inform and guide the design of the device, as well as help illustrate how the design strategy should yield fruitful results (Figures 2(a) and 4(b)). We believe a 2D modeling effort is sufficient for this purpose, however, a complete analysis of a final device would benefit from a full 3D analysis.

B. Micropillar focuser

Based on numerical simulations of resulting particle trajectories (Figure 2(a)), and the focuser geometry was designed such that suspending media and particles under 10 μm in diameter were able to slip between individual pillars, maintaining their original streamlines, and

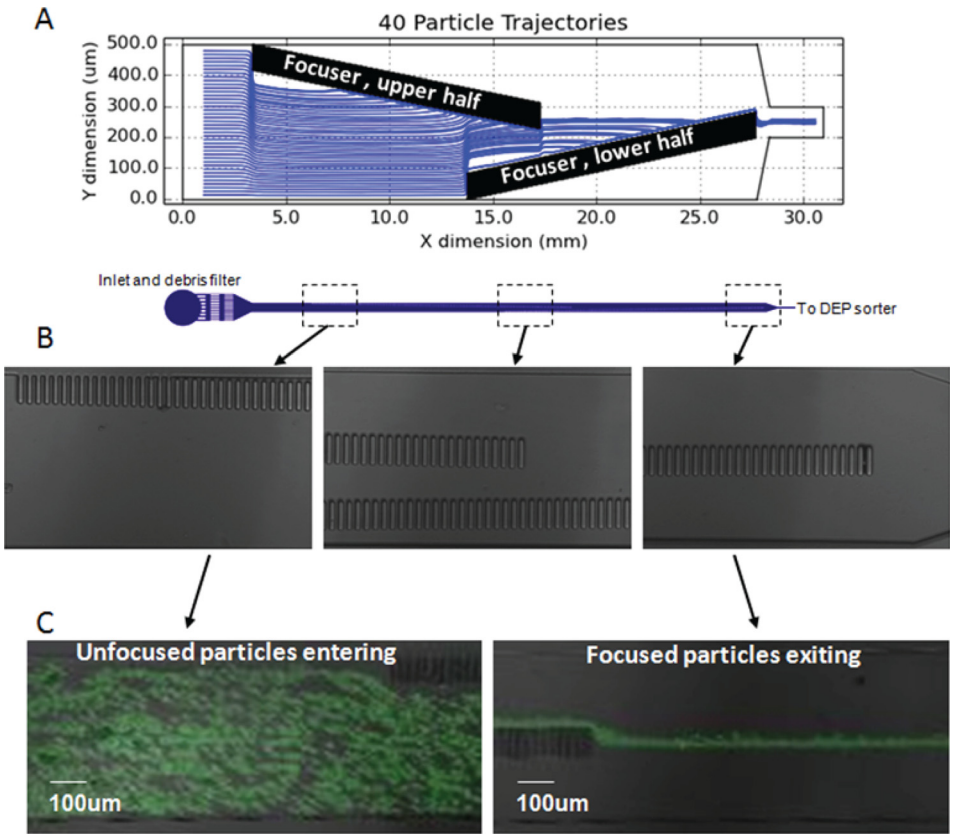

FIG. 2. Panel (a): Simulated trajectories (blue) for 40 individual 10 μm particles distributed across width of inlet as they flow through two angled rows of pillars (black). Device length is compressed to facilitate imaging. Panel (b): Entire length of passive focuser, to scale, zoomed in at start, middle, and end. Gaps between pillars allow buffer to pass through but particles are redirected towards the centerline. Panel (c): Fluorescent polystyrene beads are shown entering the focuser randomly distributed across the entirety of the channel width and exiting in a focused stream at the channel center.

consequently, due to laminar flow, their positions relative to channel width. Particles exceeding this clearance size, however, were pushed along the length of the row of pillars and settled into a single streamline by the time they exited the focuser.

As shown (Figure 2(b)), the resultant pillars were 10 μm wide, 80 μm high, spaced 10 μm apart, and spanned the entire height of the channel. The pillars were arranged in two rows, offset $\pm 0.5^\circ$ from the horizontal. This angle was chosen based on its ability to focus particles into a stream in as short a distance as possible while at the same limiting resistance to flow and not impeding particles as they shift towards the same streamline. Pillar rows at sharper angles tended to clog more easily and resulted in poorer focusing performance. A steeper angle would theoretically focus the particles over a shorter length of inlet, but in practice traps particles and creates increased resistance to flow, instead of allowing them to gently roll along the length of the rows of pillars towards a single streamline, while a shallower angle, which would theoretically minimize clogging, yields too long a footprint, exceeding the length of the entire inlet. Each of the two rows of pillars was set to terminate such that the final focused stream of particles would be positioned directly along the main flow channel's centerline.

To quantify pre-focuser efficacy, a mockup device was fabricated consisting of a straight channel with the pre-focuser positioned at the center. Viewing areas exist at positions of particle entry into and exit from the focuser. Particles are flowed into the focuser at various flow rates. Imaging was performed using an LSM780 set at 2 fps and run for 500 cycles. All frames were stacked and flattened using ImageJ (reference source); the width of the total particle distribution pre- and post-focusing was then measured digitally. The focuser was tested using 20 μm diameter particles (Figure 2(c)), the largest that can pass through the device without

confounding phenomena such as clogging and snagging to channel surfaces. The width of the total particle distribution for 20 μm particles was measured before and after passing through the focuser. A comparable result was obtained using 10 μm particles, the smallest focusable size with this geometry of pillar line.

C. Gel electrodes

The fabrication of the gel electrodes is a multistep process. A pair of planar Au/Ti traces each 1 cm $\times$ 100 μm, spaced 300 μm apart, were patterned onto a $1'' \times 3''$ glass side using photolithographic technique; wires were then soldered to these electrodes using lead free solder allowing them to interface with the external function generator. Subsequently, the PDMS channels are aligned over these planar electrodes such that the main flow channel runs between the two parallel planar electrodes, separated from each by 100 μm of clearance, while the orthogonal side channels extending from the main flow channel sit directly on top of the planar electrodes (Figure 3(a)).

To form the vertical electrodes that inject the electric field gradient into the main flow channel, the device is filled with a heated agarose 0.5% w/v saline solution at 30 mS/cm, (Figure 3(a)); for low-conductivity buffers commonly used in DEP assays, increasing the gel conductivity to 30 mS/cm minimizes voltage loss in the vertical electrodes themselves, increasing the efficiency at which the planar electrodes can produce a sufficiently strong electric field gradient across the width of the main channel. While the solution remains liquid, fresh saline is pumped into the device at 300 μl/min, clearing all accessible sections of the channel of agarose solution (Figure 3(c)). Due to laminar flow, however, the agarose saline mixture in the side channels are unaffected by this sudden influx of fresh saline and remain filled with agarose solution, which solidifies into a conductive gel as it cools below 65 °C. The gel included fluorescein for visibility under 488 nm excitation (Figure 3(d)). Small dead zones in the gel electrodes may occur when the saline is used to flush the main region; however, regions are shallow and the change to the fluidic channel and overall flow is minimal. We observed typically less than 5% change to the channel widths, with no loss of laminar flow and no trapping of particles in the dead regions.

This device uses a consistent frequency for all electrode pairs and generates field lines extending from one edge of the channel to the opposite; the electric field gradient is shaped entirely by strategic asymmetric positioning of the vertical electrodes. In contrast, most iDEP devices consist of symmetrically distributed side channels, each side connected to its own function generator with electric field lines that terminate in the same edge from which they

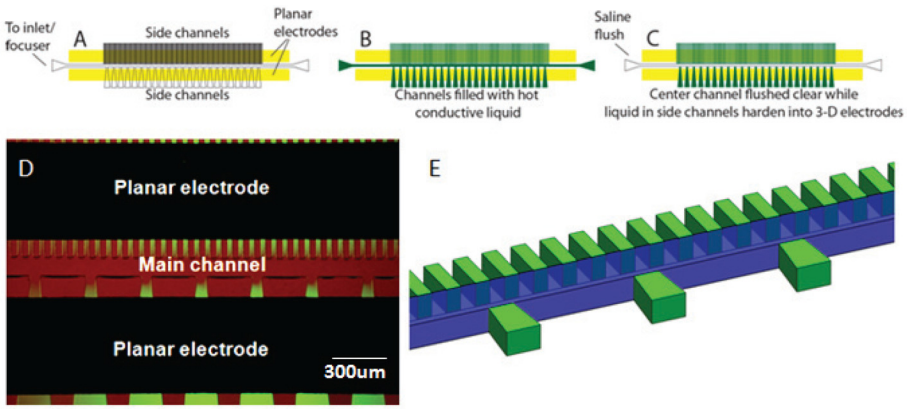

FIG. 3. Panel (a): The device (gray) is aligned over electrodes (gold); Panel (b): The device is filled with hot conductive agarose gel solution (green). Panel (c): Saline is then flushed through channel, clearing conductive liquid from the main channel but ignoring electrode sites due to laminar flow principles. After cooling and gel formation, the saline in the central channel is removed and particle suspension of interest put through the device. Panel (d): Overlay of brightfield and fluorescent image of assembled device; gel electrodes are visualized using fluorescein additive. Panel (e): 3D schematic of electrode geometry note vertical electrodes (green) are essentially flush with the walls of central channel (blue).

originate[26,36,42] and by adjusting the relative difference in signal amplitude between each side, particles are shifted across the width of the channel. The positions of our electrodes on each side of the channel were guided by drawing a schematic in COMSOL and numerically simulating the shape of the resultant fluid flow field and electric field gradient (Figure 4(a)). The resulting field information and device geometry were then imported into a program written in Python to predict particle trajectories using governing equations for dielectrophoresis and laminar flow as described above. Based on this, the specific shape and distribution of side channels as well as the strength of the signals used to energize them were derived. In the final design, electrodes on the upper (low E-field strength) edge of the device were 30 μm wide and 30 μm apart, while those on the lower (high E-field strength) edge of the device were 60 μm wide and 240 μm apart.

According to the above simulations, low dielectric constant particles, e.g., polystyrene particles, and higher dielectric constant particles, e.g., mammalian cells, in low conductivity buffer experience significantly different DEP forces at frequencies in the megahertz range, with cells experiencing a strong pDEP force while the polystyrene particles experience the opposite, yielding DEP-based separation. Theoretical trajectories for these two particle types flowing through the device at 1 μl/min are shown; the simulated device is set at 3 MHz and 50V_{pp} (Figure 4(b)). Polystyrene beads were modeled as homogeneous perfect spheres with poor conductivity and permittivity (diameter = 15 μm, $\sigma_p = 0.1$ μS/cm, $\varepsilon_p = 2.6$), while cells were modeled as perfectly spherical cytosols with physiological conductivity and permittivity (diameter = 15 μm, σ_{cyt} = 15 mS/cm, $\varepsilon_{cyt} = 80$) enclosed in a thin insulating membrane of low conductivity and permittivity (thickness = 9 nm, $\sigma_{mem} = 1.6$ μS/cm, $\varepsilon_{mem} = 20$). All particles are modeled in low-conductivity media ($\sigma_m = 150$ μS/cm, $\varepsilon_m = 78$). Electronic properties for particles and media were derived from literature.[24,73–77] Under these conditions, at 3 MHz, the CM factor for the polystyrene approaches −0.5, while the CM factor for the cells approaches +1.

IV. RESULTS AND DISCUSSION

As proof of principle for application of this device to eukaryotic cells and to demonstrate the device's ability to sort cells from a heterogeneous mixture, we employed HeLa cells

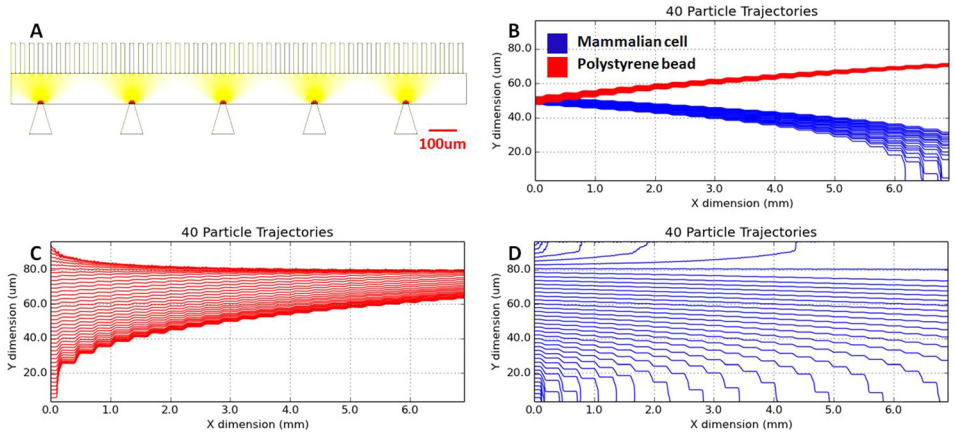

FIG. 4. Panel (a): Numerical simulation of non-uniform electric field across width of DEP sorter. Planar electrodes are located along top and bottom edges of schematic. Asymmetric distribution creates field gradient spanning width of channel (denoted in red to yellow color map of electric field). For viewing convenience, only five electric field gradient repeating units are pictured; actual device contains 23 such repeating units. All features drawn to scale. Panel (b): Calculated trajectories for low dielectric constant polystyrene particles (red) and high dielectric constant mammalian cells (blue) in low conductivity buffer passing through entire length of DEP sorter at 3 MHz and 50 V_{pp} and 1 μl/min. Schematic is compressed along x axis for visualization. Cells are attracted to the field maxima and trend towards lower edge of device while polystyrene attracted to toward the field minima and trend toward the upper edge of the device. Panels (c) and (d): Numerical simulations of particle distributions for polystyrene particles (red) and mammalian cells (blue) passing through the DEP sorter at 3 MHz, 50V_{pp}, and 1 μl/min unfocused, illustrating the benefit of an upstream pre-focuser in a DEP system.

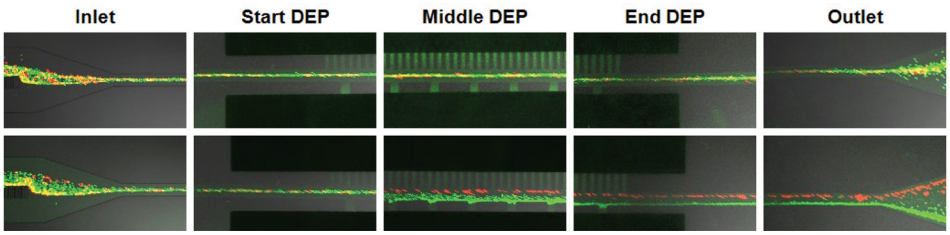

FIG. 5. Top row: Five-image sequence of mixed particle suspension (red 15 μm polystyrene beads and green HeLa cells) exiting the focuser, entering the DEP region, halfway through the DEP region, exiting the DEP region, and exiting the channel in deactivated device. Second row: Same sequence, device energized at 3MHz.

(ATCC CCL-2, Manassas, VA) and polystyrene beads. We prepared a suspension of freshly detached HeLa cells labeled with CFSE (50 μM in PBS, Sigma-Aldrich, St. Louis, MO) in low-conductivity buffer consisting of 8.5% sucrose (wt/vol), 0.3% dextrose (wt/vol), and 0.725% RPMI (vol/vol)) (150 μS/cm, pH = 7.38) at a concentration of 1×10^6 cells /ml. 15 μm polystyrene fluorescent beads (FluoSphere 580/605, Life Technologies, Eugene, OR) were then added to this mixture to a resulting concentration of 2×10^5 particles/ml. This permitted visualization of both beads and cells using standard fluorescent video microscopy (Figure 5).

To quantify separation efficiency, video footage of particles exiting the device at the channel trifurcation was collected using the LSM780 (Carl Zeiss Microscopy, Thornwood, NY) at 2 fps for 100 s and particles were counted as they passed through one of the three exits (Figure 6). As the particle mixture enters the device, it is initially focused into a stream located at the center of the flow channel; 82% of polystyrene particles and 93% of cells were focused into the center outlet, with the balance scattered into the two other channels, yielding no separation. Upon the application of a low frequency signal of 30 kHz and $30V_{pp}$, strong nDEP is experienced by the polystyrene beads, which are completely deflected into the top channel. HeLa cells display a more mixed response: the stream of cells broadens, and while most cells exit primarily through the center outlet, some are observed exiting through one of the two side outlets as well. As the frequency is increased, the polystyrene particles continue to exit through the top channel while the live cells transition gradually towards pDEP; at 3 MHz and $50V_{pp}$, near-total separation is observed with over 97% of HeLa cells and over 94% of polystyrene particles deflected into the bottom (pDEP) and top (nDEP) outlets, respectively (Figure 7). Trace amounts of each particle type passed through the center channel.

V. CONCLUSIONS

The microfluidic device presented addresses several critical issues in DEP particle sorting, namely, the decreased DEP sorting efficiency without pre-focusing of the particle stream, the dead zones commonly found in microfluidic electric field gradients, and the capacity to easily fabricate vertical 3-D electrodes using historically 2-D photolithographic methods. The design improves upon earlier liquid dielectrophoresis methods by allowing for the formation of higher conductivity 3-D gel electrodes within the device using only the properties of the laminar flow found at low Reynolds numbers. These three-dimensional electrodes were fabricated by

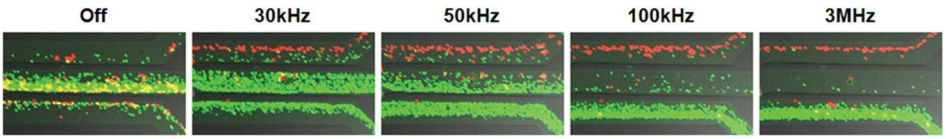

FIG. 6. Particle distribution (red 15 μm polystyrene beads and green HeLa cells) at trifurcated device outlet. Initially, nearly all particles are focused into the center channel. Upon activating the function generator at 30 kHz, polystyrene particles immediately deflect into upper channel (nDEP) while cell stream broadens into the upper and lower channels. As frequency is further increased, polystyrene particles remain in the upper channel while HeLa cells gradually transition towards the lower channel (pDEP).

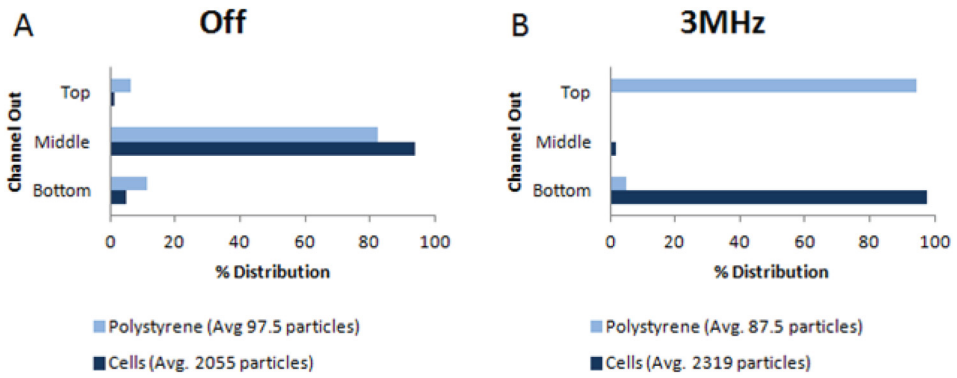

FIG. 7. Particles were counted as they exited the device through one of three outlets: undeflected particles exited through the center outlet, particles experiencing an nDEP force exited through the top, and particles experiencing a pDEP force exited through the bottom. Flow rate was 1 μl/min. Panel (a): Particle distribution in deactivated device. Panel (b): Particle distribution under $50V_{pp}$, 3 MHz signal.

strategically flowing a thermosensitive conductive liquid into the device and then selectively removing material from the main channel prior to device cooling, leaving 3-D structures shaped to generate vertical uniform and lateral non-uniform field gradients.

Initial work shows that the device can deflect particles across a wide range of frequencies and differentiate between particles of low and higher dielectric constant with high accuracy. Future work will focus on applying this sorting technology towards distinguishing subsets of live eukaryotic cells and for isolation of low population cell subsets from a larger heterogeneous mixture, e.g., hematologic cellular subsets (leukocytes) or circulating tumor cells from whole blood. This work provides an avenue to explore sorting based on detecting subtle differences in seemingly homogeneous cell populations, such as progenitor or stem cells from single tissue population, e.g., epithelium from a specific organ. Finally, future studies will be performed in buffers more conductive than the low-conductivity DEP buffer presented here; of special interest is the device's ability to sort particles at physiological conductivity, which would simplify the sample prep process and allow the device to sort using both nDEP and pDEP, across a wide range of frequencies.

ACKNOWLEDGMENTS

The authors would like to thank Amanda Ngo, Son Vuong, and Ryan Smith for preparing device graphics as well as for performing the simulation work in Python and COMSOL Multiphysics. Additionally, the authors thank Sara Saedinia, Richard Chang, and Renee Pham for assistance in fabricating and assembling all electronic components. Finally, the authors thank Amanda Laust, Trisha Westerhof, and Jo Tucker for assistance with biological assays. Special thanks to our funding agencies. This research was supported in part by the National Science's Foundation's IGERT program under Award No. 0549479, and in part by the National Cancer Institute of the National Institutes of Health under Award No. P30CA062203. The content is solely the responsibility of the authors and does not necessarily represent the official views of the National Science Foundation or the National Institutes of Health.

[1]D. R. Gossett, W. M. Weaver, A. J. Mach, S. C. Hur, H. T. K. Tse, W. Lee, H. Amini, and D. Di Carlo, "Label-free cell separation and sorting in microfluidic systems," Anal. Bioanal. Chem. **397**(8), 3249–3267 (2010).
[2]S. Nagrath, L. V. Sequit, S. Maheswaran, D. W. Bell, D. Irimia, L. Ulkus, M. R. Smith, E. L. Kwak, S. Digumarthy, A. Muzikansky, P. Ryan, U. J. Balis, R. G. Tompkins, D. A. Haber, and M. Toner, "Isolation of rare circulating tumor cells in cancer patients by microchip technology," Nature **450**, 1235–1239 (2007).
[3]A. A. S. Bhagat, H. Bow, H. W. Hou, S. J. Tan, J. Han, and C. T. Lim, "Microfluidics for cell separation," Med. Biol. Eng. Comput. **48**(10), 999–1014 (2010).
[4]H. W. Hou, A. A. S. Bhagat, A. G. Lin Chong, P. Mao, K. S. Wei Tan, J. Han, and C. T. Lim, "Deformability based cell margination—A simple microfluidic design for malaria-infected erythrocyte separation," Lab Chip **10**(19), 2605–2613 (2010).

[5]S. S. Kuntaegowdanahalli, A. A. S. Bhagat, G. Kumar, and I. Papautsky, "Inertial microfluidics for continuous particle separation in spiral microchannels," Lab Chip **9**(20), 2973 (2009).
[6]W. Sheng, O. O. Ogunwobi, T. Chen, J. Zhang, T. J. George, C. Liu, and Z. H. Fan, "Capture, release and culture of circulating tumor cells from pancreatic cancer patients using an enhanced mixing chip," Lab Chip **14**(1), 89–98 (2013).
[7]W. Sheng, T. Chen, R. Kamath, X. Xiong, W. Tan, and Z. H. Fan, "Aptamer-enabled efficient isolation of cancer cells from whole blood using a microfluidic device," Anal. Chem. **84**(9), 4199–4206 (2012).
[8]H. Morgan, M. P. Hughes, and N. G. Green, "Separation of submicron bioparticles by dielectrophoresis," Biophys. J. **77**(1), 516–525 (1999).
[9]X.-B. Wang, Y. Huang, F. F. Becker, and P. R. C. Gascoyne, "A unified theory of dielectrophoresis and travelling wave dielectrophoresis," J. Phys. D: Appl. Phys. **27**(7), 1571 (1994).
[10]L. A. Flanagan, J. Lu, L. Wang, S. A. Marchenko, N. L. Jeon, A. P. Lee, and E. S. Monuki, "Unique dielectric properties distinguish stem cells and their differentiated progeny," Stem Cells **26**(3), 656–665 (2008).
[11]L. Zheng, J. P. Brody, and P. J. Burke, "Electronic manipulation of DNA, proteins, and nanoparticles for potential circuit assembly," Biosens. Bioelectron. **20**(3), 606–619 (2004).
[12]X.-B. Wang, J. Vykoukal, F. F. Becker, and P. R. C. Gascoyne, "Separation of polystyrene microbeads using dielectrophoretic/gravitational field-flow-fractionation," Biophys. J. **74**(5), 2689–2701 (1998).
[13]B. M. Taff and J. Voldman, "A scalable addressable positive-dielectrophoretic cell-sorting array," Anal. Chem. **77**(24), 7976–7983 (2005).
[14]J. Voldman, R. A. Braff, M. Toner, M. L. Gray, and M. A. Schmidt, "Holding forces of single-particle dielectrophoretic traps," Biophys. J. **80**(1), 531–542 (2001).
[15]R. Pethig, "Review article—Dielectrophoresis: Status of the theory, technology, and applications," Biomicrofluidics **4**(2), 022811 (2010).
[16]L. Wu, L.-Y. L. Yung, and K.-M. Lim, "Dielectrophoretic capture voltage spectrum for measurement of dielectric properties and separation of cancer cells," Biomicrofluidics **6**(1), 014113 (2012).
[17]R. S. Kuczenski, H.-C. Chang, and A. Revzin, "Dielectrophoretic microfluidic device for the continuous sorting of Escherichia coli from blood cells," Biomicrofluidics **5**(3), 032005 (2011).
[18]R. Pethig and G. H. Markx, "Applications of dielectrophoresis in biotechnology," Trends Biotechnol. **15**(10), 426–432 (1997).
[19]P. R. C. Gascoyne, J. Noshari, T. J. Anderson, and F. F. Becker, "Isolation of rare cells from cell mixtures by dielectrophoresis," Electrophoresis **30**(8), 1388–1398 (2009).
[20]M. Cristofanilli, S. Krishnamurthy, C. M. Das, J. M. Reuben, W. Spohn, J. Noshari, F. Becker, and P. R. Gascoyne, "Dielectric cell separation of fine needle aspirates from tumor xenografts," J. Sep. Sci. **31**(21), 3732–3739 (2008).
[21]F. F. Becker, X. B. Wang, Y. Huang, R. Pethig, J. Vykoukal, and P. R. Gascoyne, "Separation of human breast cancer cells from blood by differential dielectric affinity," Proc. Natl. Acad. Sci. U.S.A. **92**(3), 860–864 (1995).
[22]C. Iliescu, G. Tresset, and G. Xu, "Dielectrophoretic field-flow method for separating particle populations in a chip with asymmetric electrodes," Biomicrofluidics **3**(4), 044104 (2009).
[23]S. Velugotla, S. Pells, H. K. Mjoseng, C. R. E. Duffy, S. Smith, P. D. Sousa, and R. Pethig, "Dielectrophoresis based discrimination of human embryonic stem cells from differentiating derivatives," Biomicrofluidics **6**(4), 044113 (2012).
[24]Y. Huang, R. Holzel, R. Pethig, and X.-B. Wang, "Differences in the AC electrodynamics of viable and non-viable yeast cells determined through combined dielectrophoresis and electrorotation studies," Phys. Med. Biol. **37**(7), 1499 (1992).
[25]R. Pethig, "Dielectrophoresis: Using inhomogeneous AC electrical fields to separate and manipulate cells," Crit. Rev. Biotechnol. **16**(4), 331–348 (1996).
[26]L. Wang, L. Flanagan, and A. P. Lee, "Side-wall vertical electrodes for lateral field microfluidic applications," J. Microelectromech. Syst. **16**(2), 454–461 (2007).
[27]B. Y. Park and M. J. Madou, "3-D electrode designs for flow-through dielectrophoretic systems," Electrophoresis **26**(19), 3745–3757 (2005).
[28]F. E. H. Tay, L. Yu, A. J. Pang, and C. Iliescu, "Electrical and thermal characterization of a dielectrophoretic chip with 3D electrodes for cells manipulation," Electrochim. Acta **52**(8), 2862–2868 (2007).
[29]D. Holmes, M. E. Sandison, N. G. Green, and H. Morgan, "On-chip high-speed sorting of micron-sized particles for high-throughput analysis," IEE Proc. Nanobiotechnol. **152**(4), 129–135 (2005).
[30]I.-F. Cheng, H.-C. Chang, D. Hou, and H.-C. Chang, "An integrated dielectrophoretic chip for continuous bioparticle filtering, focusing, sorting, trapping, and detecting," Biomicrofluidics **1**(2), 021503 (2007).
[31]R. Martinez-Duarte, "Microfabrication technologies in dielectrophoresis applications—A review," Electrophoresis **33**(21), 3110–3132 (2012).
[32]R. Martinez-Duarte, R. A. Gorkin III, K. Abi-Samra, and M. J. Madou, "The integration of 3D carbon-electrode dielectrophoresis on a CD-like centrifugal microfluidic platform," Lab Chip **10**(8), 1030–1043 (2010).
[33]M. del C. Jaramillo, E. Torrents, R. Martínez-Duarte, M. J. Madou, and A. Juárez, "On-line separation of bacterial cells by carbon-electrode dielectrophoresis," Electrophoresis **31**(17), 2921–2928 (2010).
[34]R. Martinez-Duarte, P. Renaud, and M. J. Madou, "A novel approach to dielectrophoresis using carbon electrodes," Electrophoresis **32**(17), 2385–2392 (2011).
[35]R. Martinez-Duarte, F. Camacho-Alanis, P. Renaud, and A. Ros, "Dielectrophoresis of lambda-DNA using 3D carbon electrodes," Electrophoresis **34**(7), 1113–1122 (2013).
[36]L. Wang, L. A. Flanagan, N. L. Jeon, E. Monuki, and A. P. Lee, "Dielectrophoresis switching with vertical sidewall electrodes for microfluidic flow cytometry," Lab Chip **7**(9), 1114–1120 (2007).
[37]T. W. Herling, T. Müller, L. Rajah, J. N. Skepper, M. Vendruscolo, and T. P. J. Knowles, "Integration and characterization of solid wall electrodes in microfluidic devices fabricated in a single photolithography step," Appl. Phys. Lett. **102**(18), 184102 (2013).
[38]J. Vykoukal, D. M. Vykoukal, S. Freyberg, E. U. Alt, and P. R. C. Gascoyne, "Enrichment of putative stem cells from adipose tissue using dielectrophoretic field-flow fractionation," Lab Chip **8**(8), 1386 (2008).
[39]R. Pethig, Y. Huang, X. Wang, and J. P. H. Burt, "Positive and negative dielectrophoretic collection of colloidal particles using interdigitated castellated microelectrodes," J. Phys. D: Appl. Phys. **25**(5), 881 (1992).

[40]S. Fiedler, S. Shirley, T. Schnelle, and G. Fuhr, Anal. Chem. **70**(9), 1909 (1998).
[41]L. Wang, J. Lu, S. A. Marchenko, E. S. Monuki, L. A. Flanagan, and A. P. Lee, "Dual frequency dielectrophoresis with interdigitated sidewall electrodes for microfluidic flow-through separation of beads and cells," Electrophoresis **30**(5), 782–791 (2009).
[42]N. Demierre, T. Braschler, P. Linderholm, U. Seger, H. van Lintel, and P. Renaud, "Characterization and optimization of liquid electrodes for lateral dielectrophoresis," Lab Chip **7**(3), 355–365 (2007).
[43]G. M. Whitesides, "The origins and the future of microfluidics," Nature **442**, 368–373 (2006).
[44]J. B. Knight, A. Vishwanath, J. P. Brody, and R. H. Austin, "Hydrodynamic focusing on a silicon chip: Mixing nanoliters in microseconds," Phys. Rev. Lett. **80**(17), 3863–3866 (1998).
[45]A. Jahn, W. N. Vreeland, M. Gaitan, and L. E. Locascio, "Controlled vesicle self-assembly in microfluidic channels with hydrodynamic focusing," J. Am. Chem. Soc. **126**(9), 2674–2675 (2004).
[46]M. Yamada, M. Nakashima, and M. Seki, "Pinched flow fractionation: Continuous size separation of particles utilizing a laminar flow profile in a pinched microchannel," Anal. Chem. **76**(18), 5465–5471 (2004).
[47]J. Yang, Y. Huang, X.-B. Wang, F. F. Becker, and P. R. C. Gascoyne, "Cell separation on microfabricated electrodes using dielectrophoretic/gravitational field-flow fractionation," Anal. Chem. **71**(5), 911–918 (1999).
[48]V. Gupta, I. Jafferji, M. Garza, V. O. Melnikova, D. K. Hasegawa, R. Pethig, and D. W. Davis, "ApoStream™, a new dielectrophoretic device for antibody independent isolation and recovery of viable cancer cells from blood," Biomicrofluidics **6**(2), 024133 (2012).
[49]R. D. Sochol, S. Li, L. P. Lee, and L. Lin, "Continuous flow multi-stage microfluidic reactors via hydrodynamic microparticle railing," Lab Chip **12**(20), 4168–4177 (2012).
[50]C. Kantak, S. Beyer, L. Yobas, T. Bansal, and D. Trau, "A 'microfluidic pinball' for on-chip generation of layer-by-layer polyelectrolyte microcapsules," Lab Chip **11**(6), 1030–1035 (2011).
[51]R. D. Sochol, R. Ruelos, V. Chang, M. E. Dueck, L. P. Lee, and L. Lin, "Continuous flow layer-by-layer microbead functionalization via a micropost array railing system," in *16th International Solid-State Sensors, Actuators and Microsystems Conference (Transducers)*, June, 2011, pp. 1761–1764.
[52]E. B. Cummings and A. K. Singh, "Dielectrophoresis in microchips containing arrays of insulating posts: Theoretical and experimental results," Anal. Chem. **75**(18), 4724–4731 (2003).
[53]T. Schnelle, T. Müller, G. Gradl, S. G. Shirley, and G. Fuhr, "Dielectrophoretic manipulation of suspended submicron particles," Electrophoresis **21**(1), 66–73 (2000).
[54]H. A. Pohl, "The motion and precipitation of suspensoids in divergent electric fields," J. Appl. Phys. **22**(7), 869–871 (1951).
[55]R. Zhou, P. Wang, and H.-C. Chang, "Bacteria capture, concentration and detection by alternating current dielectrophoresis and self-assembly of dispersed single-wall carbon nanotubes," Electrophoresis **27**(7), 1376–1385 (2006).
[56]M. Frénéa, S. P. Faure, B. Le Pioufle, P. Coquet, and H. Fujita, "Positioning living cells on a high-density electrode array by negative dielectrophoresis," Mater. Sci. Eng., C **23**(5), 597–603 (2003).
[57]P. R. C. Gascoyne and J. Vykoukal, "Particle separation by dielectrophoresis," Electrophoresis **23**(13), 1973–1983 (2002).
[58]K.-H. Han and A. B. Frazier, "Lateral-driven continuous dielectrophoretic microseparators for blood cells suspended in a highly conductive medium," Lab Chip **8**(7), 1079–1086 (2008).
[59]N.-C. Chen, C.-H. Chen, M.-K. Chen, L.-S. Jang, and M.-H. Wang, "Single-cell trapping and impedance measurement utilizing dielectrophoresis in a parallel-plate microfluidic device," Sens. Actuators, B **190**, 570–577 (2014).
[60]M. P. Hughes, *Nanoelectromechanics in Engineering and Biology* (CRC Press, 2010).
[61]S. Park, M. Koklu, and A. Beskok, "Particle trapping in high-conductivity media with electrothermally enhanced negative dielectrophoresis," Anal. Chem. **81**(6), 2303–2310 (2009).
[62]H. Shafiee, J. L. Caldwell, M. B. Sano, and R. V. Davalos, "Contactless dielectrophoresis: A new technique for cell manipulation," Biomed. Microdevices **11**(5), 997–1006 (2009).
[63]H. Shafiee, M. B. Sano, E. A. Henslee, J. L. Caldwell, and R. V. Davalos, "Selective isolation of live/dead cells using contactless dielectrophoresis (cDEP)," Lab Chip **10**(4), 438–445 (2010).
[64]G. Mernier, N. Piacentini, T. Braschler, N. Demierre, and P. Renaud, "Continuous-flow electrical lysis device with integrated control by dielectrophoretic cell sorting," Lab Chip **10**(16), 2077 (2010).
[65]C.-P. Jen and W.-F. Chen, "An insulator-based dielectrophoretic microdevice for the simultaneous filtration and focusing of biological cells," Biomicrofluidics **5**(4), 044105 (2011).
[66]A. Salmanzadeh, H. Kittur, M. B. Sano, P. C. Roberts, E. M. Schmelz, and R. V. Davalos, "Dielectrophoretic differentiation of mouse ovarian surface epithelial cells, macrophages, and fibroblasts using contactless dielectrophoresis," Biomicrofluidics **6**(2), 024104 (2012).
[67]C.-F. Chou, J. O. Tegenfeldt, O. Bakajin, S. S. Chan, E. C. Cox, N. Darnton, T. Duke, and R. H. Austin, "Electrodeless dielectrophoresis of single- and double-stranded DNA," Biophys. J. **83**(4), 2170–2179 (2002).
[68]S. Bhattacharya, T.-C. Chao, N. Ariyasinghe, Y. Ruiz, D. Lake, R. Ros, and A. Ros, "Selective trapping of single mammalian breast cancer cells by insulator-based dielectrophoresis," Anal. Bioanal. Chem. **406**(7), 1855–1865 (2014).
[69]N. Demierre, T. Braschler, R. Muller, and P. Renaud, "Focusing and continuous separation of cells in a microfluidic device using lateral dielectrophoresis," Sens. Actuators, B **132**(2), 388–396 (2008).
[70]R. C. Gallo-Villanueva, V. H. Pérez-González, R. V. Davalos, and B. H. Lapizco-Encinas, "Separation of mixtures of particles in a multipart microdevice employing insulator-based dielectrophoresis," Electrophoresis **32**(18), 2456–2465 (2011).
[71]B. H. Lapizco-Encinas, B. A. Simmons, E. B. Cummings, and Y. Fintschenko, "Dielectrophoretic concentration and separation of live and dead bacteria in an array of insulators," Anal. Chem. **76**(6), 1571–1579 (2004).
[72]Y.-K. Cho, S. Kim, K. Lee, C. Park, J.-G. Lee, and C. Ko, "Bacteria concentration using a membrane type insulator-based dielectrophoresis in a plastic chip," Electrophoresis **30**(18), 3153–3159 (2009).
[73]F. Gielen, A. J. deMello, and J. B. Edel, "Dielectric cell response in highly conductive buffers," Anal. Chem. **84**(4), 1849–1853 (2012).

[74]J. Chen, M. Abdelgawad, L. Yu, N. Shakiba, W.-Y. Chien, Z. Lu, W. R. Geddie, M. A. S. Jewett, and Y. Sun, "Electrodeformation for single cell mechanical characterization," J. Micromech. Microeng. **21**(5), 054012 (2011).
[75]Y. Shi, D. D. Ryu, and R. Ballica, "Rheological properties of mammalian cell culture suspensions: Hybridoma and HeLa cell lines," Biotechnol. Bioeng. **41**(7), 745–754 (1993).
[76]R. Pethig, "Dielectric properties of biological materials: Biophysical and medical applications," IEEE Trans. Electr. Insul. EI-**19**(5), 453–474 (1984).
[77]A. Goldup, S. Ohki, and J. F. Danielli, in *Recent Progress in Surface Science*, edited by J. F. Danielli, A. C. Riddiford, and M. D. Rosenberg (Academic Press, 1970), Vol. 3, p. 193.